ISSN 1674-1056
http://cpb.iphy.ac.cn
http://iopscience.iop.org/cpb
中国物理 B
Chinese Physics
中国物理 Chinese Physics B

Experimental investigation of vector static magnetic field detection using an NV center with a singlefirst-shell ^{13}C nuclear spin in diamond

Feng-Jian Jiang(蒋峰建), Jian-Feng Ye(叶剑锋), Zheng Jiao(焦铮), Jun Jiang(蒋军), Kun Ma(马堃), Xin-Hu Yan(闫新虎), Hai-Jiang Lv(吕海江)
Citation: Chin. Phys. B . 2018, 27(5): 057602. **doi:** 10.1088/1674-1056/27/5/057602

Journal homepage: http://cpb.iphy.ac.cn; http://iopscience.iop.org/cpb

What follows is a list of articles you may be interested in

Estimation of vector static magnetic field by an nitrogen-vacancy center with a single first-shell ^{13}C nuclear (NV-^{13}C) spin in diamond

Feng-Jian Jiang(蒋峰建), Jian-Feng Ye(叶剑锋), Zheng Jiao(焦铮), Zhi-Yong Huang(黄志永), Hai-Jiang Lv(吕海江)
Chin. Phys. B . 2018, 27(5): 057601. **doi:** 10.1088/1674-1056/27/5/057601

A dual-axis, high-sensitivity atomic magnetometer

Rujie Li(李茹杰), Wei Quan(全伟), Wenfeng Fan(范文峰), Li Xing(邢力), Zhuo Wang(王卓), Yueyang Zhai(翟跃阳), Jiancheng Fang(房建成)
Chin. Phys. B . 2017, 26(12): 120702. **doi:** 10.1088/1674-1056/26/12/120702

Spin dynamics of magnetic resonance with parametric modulation in a potassium vapor cell

Rui Zhang(张锐), Zhi-Guo Wang(汪之国), Xiang Peng(彭翔), Wen-Hao Li(黎文浩), Song-Jian Li(李松健), Hong Guo(郭弘)
Chin. Phys. B . 2017, 26(3): 030701. **doi:** 10.1088/1674-1056/26/3/030701

In-situ measurement of magnetic field gradient in a magnetic shield by a spin-exchange relaxation-free magnetometer

Fang Jian-Cheng, Wang Tao, Zhang Hong, Li Yang, Cai Hong-Wei
Chin. Phys. B . 2015, 24(6): 060702. **doi:** 10.1088/1674-1056/24/6/060702

High contrast atomic magnetometer based on coherent population trapping

Yang Ai-Lin, Yang Guo-Qing, Xu Yun-Fei, Lin Qiang
Chin. Phys. B . 2014, 23(2): 027601. **doi:** 10.1088/1674-1056/23/2/027601

Experimental investigation of vector static magnetic field detection using an NV center with a single first-shell ^{13}C nuclear spin in diamond*

Feng-Jian Jiang(蒋峰建)†, Jian-Feng Ye(叶剑锋), Zheng Jiao(焦铮), Jun Jiang(蒋军), Kun Ma(马堃), Xin-Hu Yan(闫新虎), and Hai-Jiang Lv(吕海江)‡

School of Information Engineering, Huangshan University, Huangshan 245041, *China*

(Received 9 February 2017; revised manuscript received 7 March 2018; published online 26 April 2018)

We perform a proof-of-principle experiment that uses a single negatively charged nitrogen–vacancy (NV) color center with a nearest neighbor ^{13}C nuclear spin in diamond to detect the strength and direction (including both polar and azimuth angles) of a static vector magnetic field by optical detection magnetic resonance (ODMR) technique. With the known hyperfine coupling tensor between an NV center and a nearest neighbor ^{13}C nuclear spin, we show that the information of static vector magnetic field could be extracted by observing the pulsed continuous wave (CW) spectrum.

Keywords: color centers, optical detection magnetic resonance (ODMR), magnetometer

PACS: 76.70.Hb, 76.30.Mi, 07.55.Ge **DOI:** 10.1088/1674-1056/27/5/057602

1. Introduction

Owing to its outstanding optical and electron spin individually addressable properties, negatively charged nitrogen–vacancy (NV) color center in diamond[1–3] has recently emerged as a promising candidate for a wide range of applications, such as quantum information processing (QIP),[4–11] imaging in life science,[12] and high-resolution sensing of magnetic field.[13,14] The NV-based magnetometers have been applied to an outstanding challenge in magnetic sensing, whose applications are involved from fundamental physics and material science to quantum memory and biomedical science.

The central idea for the NV-based magnetometer is that detecting the relative energy shift of degeneracy ground state induced by an external DC or AC magnetic field[13–18] can precisely extract the information (including strength and polar angle relative to NV axis) of an applied magnetic field from corresponding resonance frequencies, but the information of azimuth angle was lost due to its C_{3v} symmetry. For completely reconstructing the AC or DC vector magnetic field, ones commonly adopted a multi-NV vector magnetometer with different [111] axes NVs,[15,18] which are best to be close to each other, differing by no more than hundreds of nanometers for improving spatial resolution. Another theoretical scheme, suggested by Lee *et al.*,[17] is only to use a single high-spin (spin 3/2) system as a vector magnetometer, which may avoid the above mentioned relatively low spatial resolution.

Furthermore, nuclear spins in diamond, coupled by hyperfine interaction to nearby NV electron spin, are generally believed to contribute to its decoherence.[19,20] For detecting weakly coupled nuclear spins, dynamical decoupling (DD) pulses could be used to prolong the dephasing time of the NV electron spin,[21,22] whose sensitivity to the target nuclear spin is enhanced.[23–26] In contrast, if the hyperfine interaction is strong enough to induce resolved energy splitting, the nuclear spins could be well detected and their hyperfine tensors may be precisely determined.[27–32] Such interactions have been used to demonstrate QIP by employing NV electron and ^{13}C nuclear spins as quantum registers.[4]

In this paper, with the known hyperfine components[30–32] between an NV electron and a single nearest neighbor ^{13}C nucleus (NV–^{13}C), our proof-of-principle experiment showed that the possible directions of an applied static vector magnetic field could be determined with the assistance of the ^{13}C nuclear spin. Because of the presence of a ^{13}C nuclear spin in the first coordination shell, the symmetry of the NV center can be reduced from C_{3v} to C_s, a single mirror plane. More information of the vector field could be extracted in the continuous wave (CW) spectrums of an NV–^{13}C system compared to a single NV center. The main idea is observing the resonance spectrum lines of NV–^{13}C to determine the four transition frequencies and the Lamor splitting of sub-manifold $m_s = 0$ induced by ^{13}C nuclear spin, since their combined effects of the field strength and direction[31] together determine the corresponding resonance frequencies. The potential advantage of our method is that the NV center and the first-shell ^{13}C nucleus are only separated by the length of diamond lattice constant,

*Project supported by the National Natural Science Foundation of China (Grant Nos. 11305074, 11135002, and 11275083), the Key Program of the Education Department Outstanding Youth Foundation of Anhui Province, China (Grant No. gxyqZD2017080), and the Education Department Natural Science Foundation of Anhui Province, China (Grant No. KJHS2015B09).

†Corresponding author. E-mail: jfjiang@mail.ustc.edu.cn

‡Corresponding author. E-mail: luhj9404@mail.ustc.edu.cn

© 2018 Chinese Physical Society and IOP Publishing Ltd

and thus high spatial resolution may be achieved.

2. The detection of a static vector magnetic field with an NV–^{13}C

2.1. The Hamiltonian of NV–^{13}C system

The NV center contains a substitutional nitrogen ^{14}N atom and a vacancy in an adjacent lattice site. Its ground state has a spin triplet $S=1$ with a zero-field splitting $D=2.87$ GHz between $m_s=0$ and $m_s=\pm1$ spin sublevels. In a sample with a natural abundance of ^{13}C isotope (1.1%), a randomly placed ^{13}C nucleus (spin $I=1/2$) locates in the diamond lattice. The hyperfine splitting of ^{14}N nuclear spin (spin $I=1$) is a constant of -2.16 MHz,[28] which is insensitive to the changes of external magnetic field. Therefore, we do not take into account the ^{14}N nuclear spin temporarily, and only consider the hyperfine structure of NV electron spin coupling to the single ^{13}C nuclear spin with corresponding Hamiltonian

$$\mathcal{H}_{\mathrm{NV-^{13}C}} = DS_z^2 + \gamma_e \boldsymbol{B}\cdot\boldsymbol{S} + \gamma_n^{^{13}\mathrm{C}}\boldsymbol{B}\cdot\boldsymbol{I}^{^{13}\mathrm{C}} + \boldsymbol{S}\cdot\boldsymbol{A}\cdot\boldsymbol{I}^{^{13}\mathrm{C}}, \quad (1)$$

where $\boldsymbol{B}=B(\sin\theta\cos\phi\ \hat{\boldsymbol{x}}, \sin\theta\sin\phi\ \hat{\boldsymbol{y}}, \cos\theta\ \hat{\boldsymbol{z}})$ represents the vector magnetic field and θ and ϕ its polar and azimuthal angles in the NV frame of reference. The gyromagnetic ratios γ_e and $\gamma_n^{^{13}\mathrm{C}}$ correspond to electron and ^{13}C nuclear spin, respectively. The last term of Eq. (1) represents the NV spin coupled to a nearest neighbor ^{13}C nuclear spin, which corresponds to a magnetic dipolar hyperfine interaction $\boldsymbol{S}\cdot\boldsymbol{A}\cdot\boldsymbol{I}^{^{13}\mathrm{C}} = A_{xx}S_xI_x + A_{yy}S_yI_y + A_{zz}S_zI_z + A_{xz}S_zI_x + A_{zx}S_xI_z$. Its axis $\hat{\boldsymbol{x}}$ satisfies $A_{zy}=A_{yz}=0$ without loss of generality. Six eigenvalues E_i $(i=1\ldots,6)$ of ground state in descending order can be obtained from the relevant Hamiltonian (1) as shown schematically in Fig. 1. Eigenvectors $|E_{i=1,2,3,4}\rangle$ and $|E_{i=5,6}\rangle$ correspond to $|\pm1,\alpha_\pm\rangle$ and $|0,\beta_\pm\rangle$ of the two submanifolds $m_s=\pm1$ and $m_s=0$, respectively.

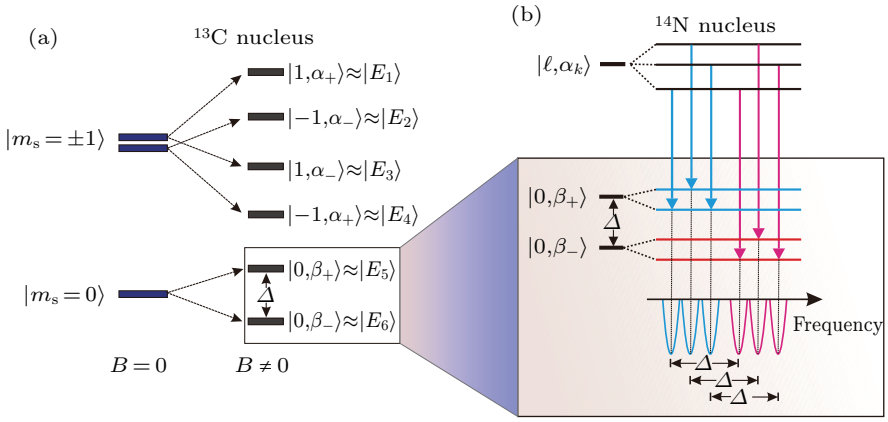


Fig. 1. (color online) (a) The energy-level diagram of NV–^{13}C center ground state. The hyperfine splitting of Δ corresponds to $m_s=0$ ground-state manifolds due to the coupling to the nearest ^{13}C nuclear spin. (b) Under the low MW power, six resonance peaks could be observed between energy levels $|\ell,\alpha_k\rangle \leftrightarrow |0,\beta_\pm\rangle$ due to hyperfine splitting of ^{14}N nuclear spin.

Applying a microwave (MW) pulse causes transitions of the system between the electron spin levels and modulates the fluorescence intensity. The spin dynamics of the ground state are relevant to microwave power, which can particularly affect the quantization axis of sub-manifold $m_s=0$. Concretely, in the case of relative low microwave power, the splitting of $m_s=0$ corresponds to two eigenstates of $|0,\beta_+\rangle$ and $|0,\beta_-\rangle$, between which the analytic form of the effective Larmor splitting obtained by second order perturbation theory

$$\Delta \approx \frac{2|\gamma_e B\sin\theta|}{D}\left(\sqrt{A_{xx}^2+A_{zx}^2}\cos^2\phi + |A_{yy}|\sin^2\phi\right)$$

reveals the direction of $\boldsymbol{B}$.[31] Correspondingly, the nuclear spin eigenstates of sub-manifold $m_s=0$ are written by $|\beta_+\rangle = \cos\frac{\theta}{2}|+1/2\rangle + e^{i\phi}\sin\frac{\theta}{2}|-1/2\rangle$ and $|\beta_-\rangle = \sin\frac{\theta}{2}|+1/2\rangle - e^{i\phi}\cos\frac{\theta}{2}|-1/2\rangle$, which depend on the direction of an applied vector field. In moderate magnetic field strength, the approximate formula of Δ conforms well to the numerical simulation based on Eq. (1).

In the remaining cases of relative high MW power, the Larmor splitting of $m_s=0$ corresponds to two linear superposition states $|0,\alpha_\pm\rangle$ of eigenstates $|0,\beta_+\rangle$ and $|0,\beta_-\rangle$, whose quantization axis of nuclear spin are realigned to a new axis defined by nuclear spin states $|\alpha_\pm\rangle$.[33] $|\alpha_\pm\rangle$ can be approximated as $|\alpha_+\rangle \approx \cos\frac{\vartheta}{2}|+\rangle + \sin\frac{\vartheta}{2}|-\rangle$ and $|\alpha_-\rangle \approx \sin\frac{\vartheta}{2}|+\rangle - \cos\frac{\vartheta}{2}|-\rangle$, where $\tan\vartheta = \frac{A_{zx}}{A_{zz}}$. In particular, the doublet transitions between $|0,\beta_\pm\rangle$ and $|\ell,\alpha_k\rangle$ ($\ell=\pm1$ and $k=\pm$) appear at the relatively low microwave power. When considering the hyperfine splitting of an ^{14}N nucleus adjacent to the vacancy, previous double transitions could be split into six resonance peaks as demonstrated schematically in Fig. 1. In contrast, high MW power leads to a single peak transition, whose corresponding frequency is almost centered between the two transition frequencies of $|0,\beta_\pm\rangle \leftrightarrow |\ell,\alpha_k\rangle$.

2.2. Experimental result and analysis

NV–^{13}C was optically addressed at room temperature by using a confocal microscope combined with a photon-counting detection system. A permanent magnet near the bulk diamond was used to apply an unknown static vector magnetic field, whose direction relative to the NV symmetry axis (z-axis) is shown schematically in Fig. 2. The electron spin resonance (ESR) transitions are driven with a microwave field applied through a 20 μm diameter copper wire directly spanned on the diamond surface.

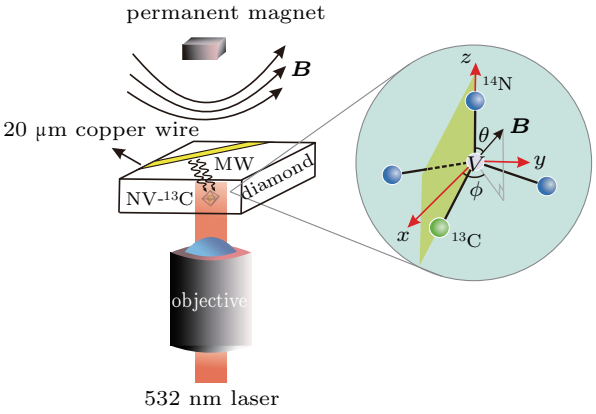


Fig. 2. (color online) The schematic of the experimental setup. A 532-nm laser was used for the initialization and readout of the NV electron spin. Control of the spin was realized through the resonant microwave pulse radiated from a 20 μm copper wire mounted on the diamond. A static vector magnetic field $\boldsymbol{B}$ is applied. NV frame of reference is defined by x, y, and z axes, where ϕ and θ represent the azimuth and polar angles with respect to the x and z axes respectively.

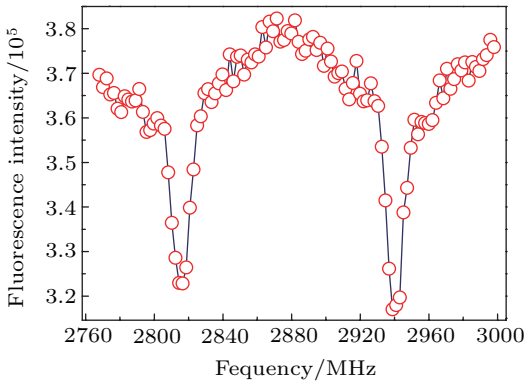


Fig. 3. (color online) An NV center with a nearest neighbor ^{13}C nucleus was identified by the zero-field splitting value 126 MHz.

In this experiment, we used the NV–^{13}C to implement the static vector magnetic field detection. As an identification of our chosen NV–^{13}C sensor, in zero-field its doublet splitting should be about 130 MHz.[34] For this purpose, the experimental optical detection magnetic resonance (ODMR) spectra was firstly applied in zero-field to determine the two resonance frequencies. As shown in Fig. 3, at room temperature the spectral lines of the chosen NV–^{13}C defect exhibit about 126 MHz zero-field splitting, which conforms to the numerical simulation of 131($\pm$9) MHz based on hyperfine tensors Table 1 and Hamiltonian Eq. (1). The deviation of zero-field splitting comes from $\pm\alpha_{ij}$ of hyperfine components. Concrete analysis can be seen in Appendix B.

Under the detected vector magnetic field, experimental pulsed CW spectrums of NV–^{13}C are demonstrated in Fig. 4. It should be noted that magnetic dipolar interactions with a bath of nuclear spin fundamentally affect the full width at half maximum (FWHM) Γ of CW spectrum, which is limited by the inhomogeneous dephasing rate. Furthermore, the FWHM could also be affected by power broadening, which is from the laser light used for polarizing electron spin and MW field used for spin rotation. Thus, the laser intensity and MW power should be appropriately reduced in experiment for achieving a narrower linewidth.[35] Specifically, in Figs. 4(a1)–4(a4) MW power was reduced by -10 dB with relevant duration of π pulse 1000–1200 ns. Due to the coupling with the ^{13}C and ^{14}N nucleus, the resonance fluorescence spectrum in each one of Figs. 4(a1)–4(a4) shows six resonance peaks, for which Γ is about 1.2 MHz. It seems like each one of the Figs. 4(a1)–4(a4) has five peaks, because the middle two ones of these six resonance frequencies as schematically depicted in Fig. 1 are too close to each other. In addition, the fluorescence intensities of spectral lines as shown in Fig. 4 are asymmetric. The reason is that the transition probabilities between the two transition matrices of $|\langle E_5|S_x|E_j\rangle|^2$ and $|\langle E_6|S_x|E_j\rangle|^2$ $(j=1,2,3,4)$ are different. Based on the transition matrix, we could find that the relative fluorescence intensity of the doublet transition should depend on polar angle θ for a determined hyperfine tensor of an NV–^{13}C system.

The four transition frequencies $\nu_{1,2,3,4}$ are sensitive to the changes of polar angle θ, compared to its insensitivity of the changes of azimuth angle ϕ. However, the Larmor splitting Δ is sensitive to the changes of ϕ. Thus, to precisely detect the vector magnetic field, both the two factors of $\nu_{1,2,3,4}$ and Δ as listed in Table 1 should be taken into account to extract the information of magnetic strength and possible directions by a method akin to maximum likelihood estimation[15] (seen also in Appendix C). Taking the spectral linewidth and known hyperfine component deviation α_{ij} into consideration by the numerical search program, we determined the eight possible directions of detected $\boldsymbol{B}$ as listed in Table 2. Due to the lack of a calibrated magnetic field in our experimental apparatus, we only estimated the errors listed in Table 2. The spectral broadening determines the spatial resolution of the detected magnetic field as the simulation analysis in Appendix D. Finally, it should be noted that our scheme of detecting the vector field by observing CW spectrums is only suitable for magnetic field strength being less than 200 Gs. Otherwise, it will dramatically influence the fluorescence intensity of the NV center.

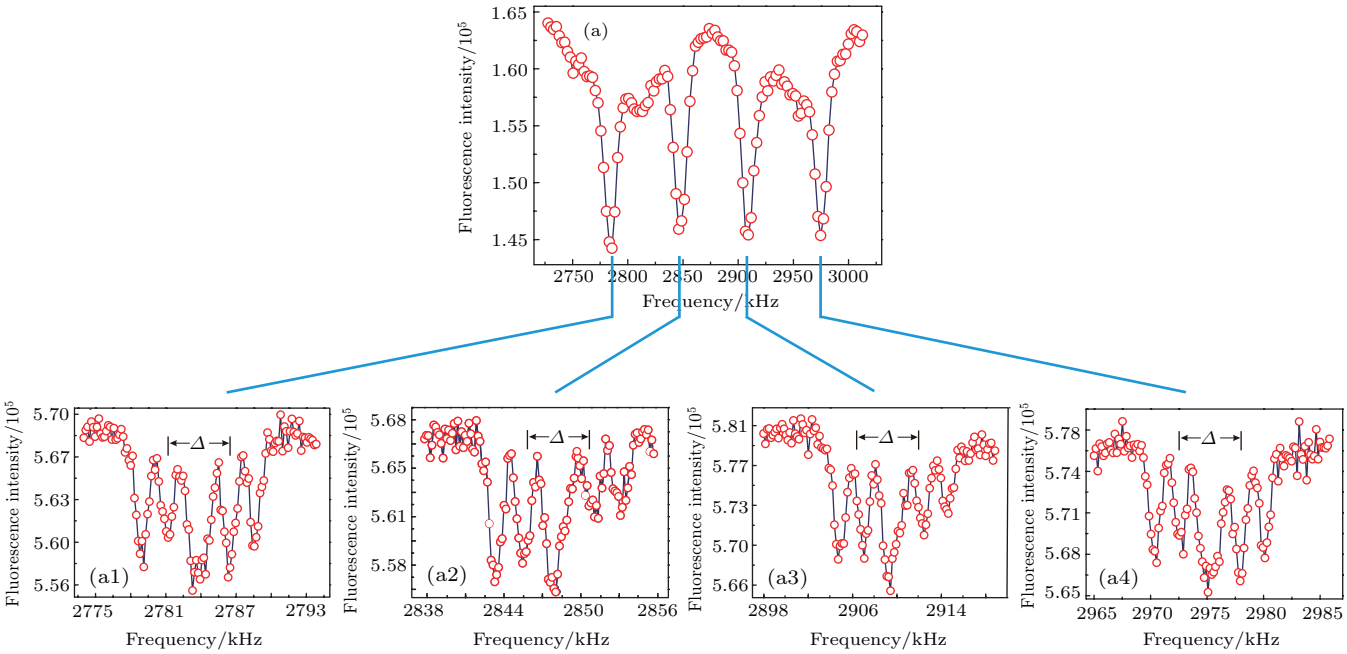


Fig. 4. (color online) Experimental data demonstrate the hyperfine structure of NV–^{13}C via a change in fluorescence detection with 100 sampling points. (a) At relatively high power, the chosen NV–^{13}C indicates four resonance frequencies due to hyperfine coupling with a single ^{13}C nucleus for a detected magnetic field configuration. (a1)–(a4) The relatively low microwave power reveals doublet transitions of each corresponding resonance line in panel (a) and hyperfine splitting induced by ^{14}N nucleus. The hyperfine splitting Δ of ground state $m_s = 0$ induced by ^{13}C nucleus is 5.3 MHz. The FWHM Γ of CW spectra is about 1.2 MHz.

Table 1. Four experimental resonance frequencies $\nu_{1,2,3,4}$ and Larmor splitting Δ obtained by fitting experimental data.

Resonance frequency	ν_1/GHz	ν_2/GHz	ν_3/GHz	ν_4/GHz	Δ/MHz
Experimental data	2.974	2.909	2.847	2.784	5.3
FWHM of CW spectra			1.2 MHz		

Table 2. Experimental result for the detected static vector magnetic field.

The parameters of $\boldsymbol{B}$	Experimental results
B_0/Gs	19.3(±1.3)
θ_0/rad	1.03(±0.04), 2.11(±0.04)
ϕ_0/rad	1.25(±0.29), 1.89(±0.29)
	4.39(±0.29), 5.03(±0.29)

3. Conclusion

In this paper, we implemented a proof-of-principle experiment that an NV center with a first-shell ^{13}C nuclear spin was applied to reconstruct the three dimensional magnetic field vector by a single NV center. Based on accurate hyperfine tensors between an electron and a single nearest-neighbor ^{13}C nucleus, by observing its hyperfine splitting spectrums induced by both ^{14}N and ^{13}C nucleus, we could obtain the desired information of the strength and eight possible directions. Different to the other published method that uses three NV centers with different axis directions, our method has the advantage that one could use a single NV center so that it can potentially combine with the nanoscale magnetic imaging to achieve the ultimate resolution. We hope that in future work it may be possible to further improve the spatial resolution by reduction of spectral broadening.

Appendix A: Candidate hyperfine tensors of NV–^{13}C

In the NV frame of reference, the symmetric hyperfine tensor

$$\boldsymbol{A} = \begin{pmatrix} A_{xx} & 0 & A_{xz} \\ 0 & A_{yy} & 0 \\ A_{zx} & 0 & A_{zz} \end{pmatrix} \text{MHz}, \tag{A1}$$

associated with the nearest ^{13}C coupling to NV spin was determined in Ref. [32], where $A_{i,j}$ with errors $\pm\alpha_{ij}$ $(i, j = x, y, z)$ is the component of $\boldsymbol{A}$. Due to the C_s symmetry of NV–^{13}C, the specific parameters are listed in Table 3, in which the signs of A_{xz} can be positive or negative, linked by a π rotation transformation around the z axis.

Table 3. Hyperfine tensors for NV–^{13}C (in units of MHz).

	$A_{xx}(\pm\alpha_{xx})$	$A_{yy}(\pm\alpha_{yy})$	$A_{zz}(\pm\alpha_{zz})$	$A_{xz}(\pm\alpha_{xz})$
$\boldsymbol{A}_1$	189.3(±1.1)	128.4(±1.0)	128.9(±4.3)	±24.1(±1.2)
$\boldsymbol{A}_2$	–189.3(±1.1)	128.4(±1.0)	–128.9(±4.3)	∓24.1(±1.2)
$\boldsymbol{A}_3$	–163.0(±2.4)	–128.4(±1.0)	85.7(±3.3)	∓99.3(±2.8)
$\boldsymbol{A}_4$	163.0(±2.4)	–128.4(±1.0)	–85.7(±3.3)	±99.3(±2.8)

Appendix B: Zero-field splitting taking into account the deviations of hyperfine components

We have the zero-field Hamiltonian of Eq. (1)

$$\begin{aligned}\mathcal{H}_{\text{NV}-^{13}\text{C}} = {} & DS_z^2 + A_{xx}S_xI_x + A_{yy}S_yI_y + A_{zz}S_zI_z \\ & + A_{xz}S_zI_x + A_{zx}S_xI_z,\end{aligned} \tag{B1}$$

and take into account that the deviation $\pm\alpha_{ij}$ of hyperfine component A_{ij} leads to the marked difference of zero-field splitting

as shown in Fig. 5. Each hyperfine component in Eq. (B1) is set between $A_{ij}-\alpha_{ij}$ and $A_{ij}+\alpha_{ij}$ with step size $\alpha_{ij}/4$. Traversal based on various deviation combinations mentioned above reveals the range of zero-field splitting values.

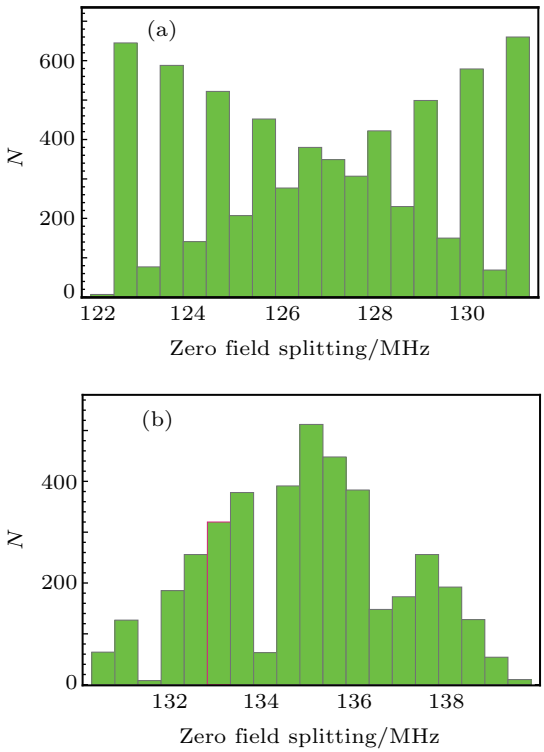


Fig. 5. (color online) The range of zero field splitting taking into account the deviations $\pm\alpha_{ij}$ of eight possible hyperfine tensors. Horizontal coordinate represents possible hyperfine splitting values for $B=0$. Vertical coordinate N represents the number corresponding to each interval value of zero field splitting. (a) Hyperfine tensors corresponding to $\boldsymbol{A}_1$ and $\boldsymbol{A}_2$. (b) Hyperfine tensors corresponding to $\boldsymbol{A}_3$ and $\boldsymbol{A}_4$.

Appendix C: Error analysis of experiment

Our computer programs implemented a numerical search procedure to match both the four target experimental resonance frequencies ν_i $(i=1,2,3,4)$ and Larmor splitting Δ according to

$$\xi(\theta,\phi,B)=\sum_{i=1,2,3,4}|E_i-(E_5+E_6)/2-\nu_i| +|E_5-E_6-\Delta|. \tag{C1}$$

One could pick the parameters θ_0, ϕ_0, and B_0 satisfying $\xi_{\min}(\theta_0,\phi_0,B_0)=\min_{\theta,\phi,B}\xi(\theta,\phi,B)$ that minimize Eq. (C1), compared to other choices of parameters. The search range of orientation parameters θ and ϕ was set to $[0,\pi]$ and $[0,2\pi]$, respectively. By taking into account the FWHM $\Gamma\approx 1.2$ MHz of CW spectra, we introduced random measurement error with a random real number $\varepsilon_\Gamma\in(-\Gamma/2,\Gamma/2)$. The formula of Eq. (C1) could be rewritten as

$$\xi(\theta,\phi,B)=\sum_{i=1,2,3,4}|E_i-(E_5+E_6)/2-(\nu_i+\varepsilon_\Gamma)| +|E_5-E_6-(\Delta+\varepsilon_\Gamma)|. \tag{C2}$$

Appendix D: Error tolerance of our scheme

As an example, based on Eq. (C2), we simulate the detected magnetic field $\boldsymbol{B}$ with preset target parameters $\phi=2.1$ rad, $\theta=1.04$ rad, and $B=22.7$ Gs without loss of generality. The errors of these detected parameters could be effectively reduced through narrowing the Γ of CW spectra as simulated in Fig. 6.

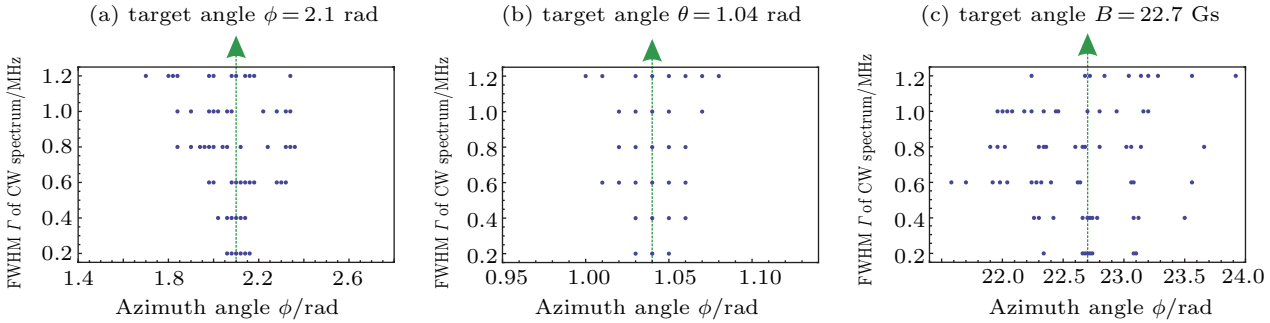


Fig. 6. (color online) The target direction and strength of magnetic field $\boldsymbol{B}$ are set to $\phi=2.1$ rad, $\theta=1.04$ rad, and $B=22.7$ Gs, respectively. The random error ε_Γ defined in Appendix C is limited within $(-\Gamma/2,\Gamma/2)$, in which 15 random number of each relevant Γ (including $\Gamma=0.2,0.4,\ldots,1.2$ MHz) are introduced in our numerical search program.

Acknowledgment

We thank Ke-Biao Xu and Peng-Fei Wang for our helpful discussions.

References

[1] Gruber A, Drabenstedt A, Tietz C, Fleury L, Wrachtrup J and von Borczyskowski C 1997 *Science* **276** 2012

[2] Jelezko F, Gaebel T, Popa I, Domhan M, Gruber A and Wrachtrup J 2004 *Phys. Rev. Lett.* **93** 130501

[3] Jelezko F, Gaebel T, Popa I, Gruber A and Wrachtrup J 2004 *Phys. Rev. Lett.* **92** 076401

[4] Neumann P, Mizuochi N, Rempp F, Hemmer P, Watanabe H, Yamasaki S, Jacques V, Gaebel T, Jelezko F and Wrachtrup J 2008 *Science* **320** 1326

[5] Jiang L, Hodges J S, Maze J R, Maurer P, Taylor J M, Cory D G, Hemmer P R, Walsworth R L, Yacoby A, Zibrov A S and Lukin M D 2009 *Science* **326** 267

[6] Shi F Z, Rong X, Xu N Y, Wang Y, Wu J, Chong B, Peng X H, Kniepert J, Schoenfeld R, Harneit W, Feng M and Du J F 2010 *Phys. Rev. Letts.* **105** 040504

[7] Maurer P C, Kucsko G, Latta C, Jiang L, Yao N Y, Bennett S D, Pastawski F, Hunger D, Chisholm N, Markham M, Twitchen D J, Cirac J I and Lukin M D 2012 *Science* **336** 1283

[8] Rong X, Geng J P, Wang Z X, Zhang Q, Ju C Y, Shi F Z, Duan C K and Du J F 2014 *Phys. Rev. Lett.* **112** 050503

[9] Gurudev Dutt M V, Childress L, Jiang L, Togan E, Maze J, Jelezko F, Zibrov A S, Hemmer P R and Lukin M D 2007 *Science* **316** 1312

[10] Maurer P C, Kucsko G, Latta C, Jiang L, Yao N Y, Bennett S D, Pastawski F, Hunger D, Chisholm N, Markham M, Twitchen D J, Cirac J I and Lukin M D 2012 *Science* **336** 1283

[11] Shim J H, Niemeyer I, Zhang J and Suter D 2013 *Phys. Rev. A* **87** 012301

[12] Shi F Z, Zhang Q, Wang P F, Sun H B, Wang J, Rong X, Chen M, Ju C Y, Reinhard F, Chen H W, Wrachtrup J, Wang J F and Du J F 2015 *Science* **347** 1135

[13] Maze J R, Stanwix P L, Hodges J S, Hong S, Taylor J M, Cappellaro P, Jiang L, Gurudev Dutt M V, Togan E, Zibrov A S, Yacoby A, Walsworth R L and Lukin M D 2008 *Science* **455** 644

[14] Balasubramanian G, Chan I Y, Kolesov R, AlHmoud M, Tisler J, Shin C, Kim C D, Wojcik A, Hemmer P R, Krueger A, Hanke T, Leitenstorfer A, Bratschitsch R, Jelezko F and J Wrachtrup 2008 *Nature* **455** 648

[15] Wang P F, Yuan Z H, Huang P, Rong X, Wang M Q, Xu X K, Duan C K, Ju C Y, Shi F Z and Du J F 2015 *Nat. Commun.* **6** 6631

[16] Xu N Y, Jiang F J, Tian Y, Ye J F, Shi F Z, Lv H J, Wang Y, Wrachtrup J and Du J F 2016 *Phys. Rev. B* **93** 161117

[17] Lee S Y, Niethammer M and Wrachtrup J 2015 *Phys. Rev. B* **92** 115201

[18] Maertz B J, Wijnheijmer A P, Fuchs G D, Nowakowski M E and Awschalom D D 2010 *Appl. Phys. Lett.* **96** 092504

[19] Hanson R, Dobrovitski V V, Feiguin A E, Gywat O and Awschalom D D 2008 *Science* **320** 352

[20] Maze J R, Taylor J M and Lukin M D 2008 *Phys. Rev. B* **78** 094303

[21] Childress L, Gurudev Dutt M V, Taylor J M, Zibrov A S, Jelezko F, Wrachtrup J, Hemmer P R and Lukin M D 2006 *Science* **314** 281

[22] Xu X K, Wang Z X, Duan C K, Huang P, Wang P F, Wang Y, Xu N Y, Kong X, Shi F Z, Rong X and Du J F 2012 *Phys. Rev. Lett.* **109** 070502

[23] Kolkowitz S, Unterreithmeier Q P, Bennett S D and Lukin M D 2012 *Phys. Rev. Lett.* **109** 137601

[24] Shi F Z, Kong X, Wang P F, Kong F, Zhao N, Liu R B and Du J F 2014 *Nat. Phys.* **10**

[25] Ma W C, Shi F Z, Xu K B, Wang P F, Xu X K, Rong X, Ju C Y, Duan C K, Zhao N and Du J F 2015 *Phys. Rev. A* **92** 033418

[26] Zhao N, Hu J L, Ho S W, Wan J T K and Liu R B 2011 *Nat. Nanotechnol.* **6** 242

[27] Loubser J H N and van Wyk J A 1977 *Diamond Research* (Ascot: De Beers Industrial Diamond Division) pp. 11–14

[28] Felton S, Edmonds A M, Newton M E, Martineau P M, Fisher D, Twitchen D J and Baker J M 2009 *Phys. Rev. B* **79** 075203

[29] Dreau A, Maze J R, Lesik M, Roch J F and Jacques V 2012 *Phys. Rev. B* **85** 134107

[30] Simanovskaia M, Jensen K, Jarmola A, Aulenbacher K, Manson N and Budker D 2013 *Phys. Rev. B* **87** 224106

[31] Shim J H, Nowak B, Niemeyer I, Zhang J, Brandäo F D and Suter D arXiv: 13070257v2 [quant-ph]

[32] Rao K R K and Suter D 2016 *Phys. Rev. B* **94** 060101

[33] Ivarez G A A, Bretschneider C O, Fischer R, London P, Kanda H, Onoda S, Isoya J, Gershoni D and Frydman L 2015 *Nat. Commun.* **6** 8456

[34] Jelezko F, Gaebel T, Popa I, Domhan M, Gruber A and Wrachtrup J 2014 *Phys. Rev. Letts.* **93** 130501

[35] Dreau A, Lesik M, Rondin L, Spinicelli P, Arcizet O, Roch J F and Jacques V 2011 *Phys. Rev. B* **84** 195204